

# TiGer: Self-Supervised Purification for Time-evolving Graphs

Hyeonsoo Jo<sup>1</sup>[0000-0002-9281-8672], Jongha Lee<sup>1</sup>[0000-0001-7197-3529], Fanchen Bu<sup>2</sup>[0000-0003-0497-3902], and Kijung Shin<sup>1</sup>[0000-0002-2872-1526] (✉)

<sup>1</sup> Kim Jaechul Graduate School of AI, KAIST, Seoul, Republic of Korea

<sup>2</sup> School of Electrical Engineering, KAIST, Daejeon, Republic of Korea

{hsjo, jhsk777, boqvezen97, kijungs}@kaist.ac.kr

**Abstract.** Time-evolving graphs, such as social and citation networks, often contain noise that distorts structural and temporal patterns, adversely affecting downstream tasks, such as node classification. Existing purification methods focus on static graphs, limiting their ability to account for critical temporal dependencies in dynamic graphs. In this work, we propose TiGER (**T**ime-evolving **G**raph **purifi****E**R), a self-supervised method explicitly designed for time-evolving graphs. TiGER assigns two different sub-scores to edges using (1) self-attention for capturing long-term contextual patterns shaped by both adjacent and distant past events of varying significance and (2) statistical distance measures for detecting inconsistency over a short-term period. These sub-scores are used to identify and filter out suspicious (i.e., noise-like) edges through an ensemble strategy, ensuring robustness without requiring noise labels. Our experiments on five real-world datasets show TiGER filters out noise with up to 10.2% higher accuracy and improves node classification performance by up to 5.3%, compared to state-of-the-art methods.

**Keywords:** Graph Purification · Dynamic Graphs · Robust Learning.

## 1 Introduction

Many real-world systems evolve over time, such as social networks and citation networks, resulting in a need for efficient methods to process and analyze these changes. Such systems are commonly modeled as *time-evolving graphs*.

*Noise* is a prevalent challenge in time-evolving graphs [6,11,25]. For instance, social networks may contain noisy interactions from spam accounts or erroneous users, distorting graph structures. As graphs grow in scale, noise increases correspondingly, amplifying its adverse impact on downstream task performance and demanding robust methods to mitigate it effectively.

*Graph purification* enhances the quality of graph data by detecting and mitigating noise that deviates from underlying *patterns* (i.e., normal behaviors). It typically measures a similarity of node pairs that form edges in the graph, identifying edges with low similarity as noise. Existing methods for measuring similarity can be broadly categorized into local similarity-based and global

similarity-based approaches, depending on the scope of the structural information they utilize. Local similarity-based methods, such as the Jaccard Coefficient [16] and the Adamic-Adar Index [20], evaluate node-pair similarity based on local neighborhood information. Global similarity-based approaches, such as singular value decomposition (SVD), leverage global structural properties to remove noise-like edges. Despite their effectiveness, these techniques are designed for *static graphs*, where only *structure patterns* are considered.

To the best of our knowledge, we are the first to consider graph purification on time-evolving graphs. This task presents unique challenges due to the dynamic nature of these graphs, where *temporal patterns* play a critical role in distinguishing noise from meaningful connections [1, 7, 18]. Specifically, each time-evolving graph can be seen as a sequence of static snapshots with temporal dependencies between each other. We can use graph purification methods for static graphs on different snapshots, but such a naive way treats different snapshots as independent and overlooks temporal patterns. This limitation highlights the need for a graph purification method explicitly considering temporal patterns.

In this work, we propose TiGER (**T**ime-evolving **G**raph purifier), a self-supervised graph-purification method explicitly designed for time-evolving graphs. TiGER comprehensively captures two different categories of temporal patterns that are common in real-world time-evolving graphs: (1) *long-term patterns* (e.g., contextual patterns shaped by both adjacent and distant past events of varying significance) and (2) *short-term patterns* (e.g., consistency across consecutive time steps over a short period). Specifically, two different sub-scores are assigned to edges using (1) self-attention for capturing long-term patterns and (2) statistical distance measures for detecting unusual deviations from short-term patterns, respectively. Those two sub-scores are combined via an ensemble strategy, together with a third proximity-based sub-score, to ensure robust and efficient purification across time steps, all without noise labels.

Our contributions are summarized as follows:

- **Novel Problem:** To the best of our knowledge, we are the first to consider graph purification on time-evolving graphs, where unique challenges of incorporating temporal patterns are involved.
- **Effective Method:** We propose TiGER, a self-supervised purification method for time-evolving graphs. TiGER leverages long-term and short-term temporal patterns to effectively identify noise, without requiring label supervision.
- **Empirical Validation:** Experiments on five real-world datasets show that TiGER filters out noise with up to 10.2% higher accuracy and achieves 5.3% higher node classification accuracy, compared to state-of-the-art methods.

For **reproducibility**, we make our code and datasets publicly available at [5].

## 2 Preliminaries and Related Work

### 2.1 Background

A *static graph*  $G = (V, E)$  is defined by its node set  $V$  and edge set  $E \subseteq \{(v_i, v_j) : v_i, v_j \in V\}$ . A *time-evolving graph* can be represented as a sequence

of static graphs  $G^{(t)} = (V^{(t)}, E^{(t)})$  across time steps  $t \in \{1, \dots, T\}$ , i.e.,  $\mathcal{G} = \{G^{(1)}, G^{(2)}, \dots, G^{(T)}\}$ . In this work, a node or edge that appears at time step  $t$  is treated as present in all subsequent time steps, i.e.,  $V^{(t)} \subseteq V^{(t')}$  and  $E^{(t)} \subseteq E^{(t')}$ , for any  $t < t'$ . Let  $\Delta G^{(t)} = (\Delta V^{(t)}, \Delta E^{(t)})$  denote the change at time step  $t$  with new nodes  $\Delta V^{(t)} = V^{(t)} \setminus V^{(t-1)}$  and new edges  $\Delta E^{(t)} = E^{(t)} \setminus E^{(t-1)}$ .

## 2.2 Graph Purification

Graph purification, a common pre-processing step in graph analysis, removes noisy edges from graph data by measuring a similarity between adjacent nodes [12,17,19,2]. Similarity measurement can be *local*, using metrics like the Jaccard Coefficient [16] and Adamic-Adar Index [20], or *global*, considering the entire graph structure, e.g., through singular value decomposition (SVD) [3]. Although effective, most graph purification methods are designed for static graphs and overlook temporal patterns crucial for identifying noise.

A related approach, graph augmentation, adds edges between similar nodes based on positions [8,9] or labels [2] in both static and dynamic graphs. Recent work [9] models temporal dependencies through a weighted summation of high-order node proximities over time. In our experiments, we adapt such augmentation methods for purification by removing edges between dissimilar nodes.

## 2.3 Temporal Patterns

*Temporal patterns* in time-evolving graphs are classified into long-term (contextual) and short-term (consistency) patterns.

*Long-term patterns* capture temporal dependencies over extended periods, shaped by both recent and distant past events. For example, in a coauthorship network, these patterns may reveal ongoing collaborations within a research group over several years. Dynamic graph neural networks (DGNNs) [13,15,14] capture such patterns using modules like RNNs or self-attention [22].

In contrast, *short-term patterns* reflect consistent behaviors over a short period. In social networks, users often interact with the same neighbors over short periods, showing consistency in interaction patterns. Many DGNN studies [10,21,24,26] exploit this consistency, assuming that node representations evolve gradually with minimal short-term changes.

## 3 Proposed Method: TiGER

In this section, we introduce our proposed method, TiGER (**T**ime-evolving **G**raph purifi**E**R), for dynamic graph purification. TiGER uses both long-term and short-term patterns to assign edge scores without ground-truth noise labels. It consists of two dedicated modules: (Module 1; Sec. 3.2) long-term module  $M_L$  with self-attention to capture contextual patterns over long periods, and (Module 2; Sec. 3.3) short-term module  $M_S$  that computes statistical distances to detect

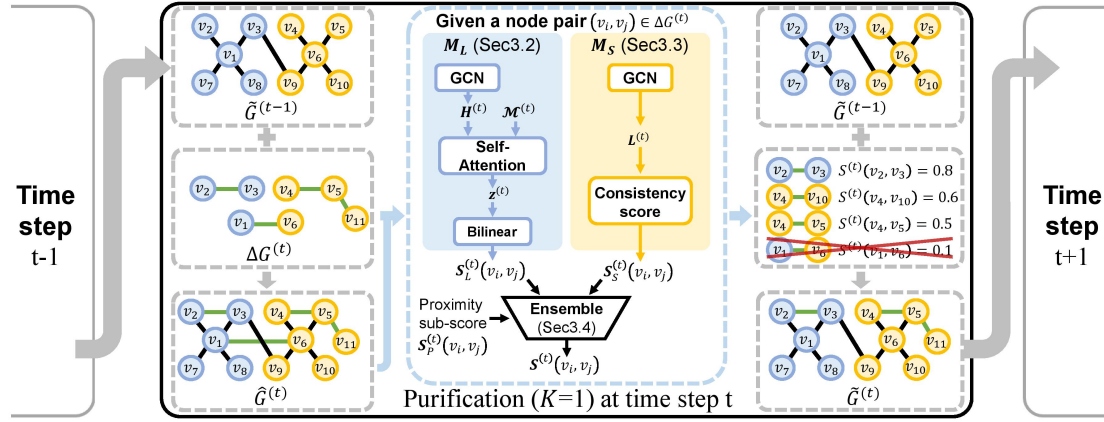


Fig. 1: Overall process of graph purification using TiGER at each time step  $t$ .

deviations from consistency over short periods. TiGER then ensembles the sub-scores from both modules to obtain the final purification scores (Sec. 3.4), where an extra proximity-based sub-score is used to enhance robustness.

### 3.1 Overview

As illustrated in Fig. 1, the overall process of graph purification on time-evolving graphs using TiGER is iterative on each time step. At each time step  $t$ , let  $\tilde{G}^{(t-1)}$  denote the *purified graph* at the previous time step  $t-1$ . We first add all incoming nodes and edges (see Sec. 2) to obtain the *unpurified graph*  $\hat{G}^{(t)} := \tilde{G}^{(t-1)} \cup \Delta G^{(t)}$ , and then we identify noise edges among the incoming edges  $\Delta E^{(t)}$ .<sup>3</sup> Here, we only consider  $\Delta E^{(t)}$  as candidate edges for efficiency since noise edges in  $\tilde{G}^{(t-1)}$  have already been purified in previous time steps. Each candidate edge  $(v_i, v_j) \in \Delta E^{(t)}$  is given a *purification score*  $S^{(t)}(v_i, v_j)$ , and the bottom- $K$  edges w.r.t. the scores are removed.

### 3.2 Long-term Module $M_L$

The long-term module  $M_L$  captures temporal dependencies over extended periods (e.g., contextual patterns) and detects noise-like edges that deviate from these patterns, by using self-attention [22].

At each time step  $t$ , we first extract intrinsic information from the unpurified graph  $\hat{G}^{(t)}$  and node attributes  $X^{(t)}$  by computing the node embedding matrix  $\mathbf{H}^{(t)}$  using a graph convolutional network (GCN)  $f_L^{(t)}$  i.e.,  $\mathbf{H}^{(t)} = f_L^{(t)}(\hat{G}^{(t)}, \mathbf{X}^{(t)})$ .<sup>4</sup> To incorporate long-term temporal dependencies, for each node, we consider the embeddings from all the previous time steps. For each node  $v_i \in V^{(t)}$ , let  $\mathbf{h}_i^{(t)}$  denote its embedding at time step  $t$ , and let  $\mathcal{M}_i^{(t)}$  denote the memory set of its past embeddings, i.e.,  $\mathcal{M}_i^{(t)} = \{\mathbf{h}_i^{(t)}, \mathbf{h}_i^{(t-1)}, \dots, \mathbf{h}_i^{(k_i)}\}$ ,

<sup>3</sup> For  $t = 1$ , we see  $\tilde{G}^{(1)}$  as an initial graph  $G^{(1)}$ .

<sup>4</sup> We use GCNs as a natural choice for graphs, while any suitable model can be used.

**Algorithm 1:** Consistency score

---

**Input:** (1) an edge  $(v_i, v_j)$ , (2) a time step  $t$ , (3) a surrogate GCN model  $f_S^{(t)}$ , (4) an unpurified graph  $\hat{G}^{(t)}$ , (5) a node features  $\mathbf{X}^{(t)}$ .

**Output:** consistency score of the given edge  $(v_i, v_j)$ .

- 1  $\mathbf{L}^{(t)} \leftarrow f_S^{(t)}(\hat{G}^{(t)}, \mathbf{X}^{(t)})$ ;
- 2  $K_i \leftarrow \{KL\text{-divergence}(\mathbf{l}_i^{(t)}, \mathbf{l}_k^{(t)}) | v_k \in N_i^{(t)}\}$ ;
- 3  $\mu_i, \sigma_i \leftarrow \text{mean}(K_i), \text{stdev}(K_i)$ ;
- 4  $Z_i^{(t)} \leftarrow \frac{|KL\text{-divergence}(\mathbf{l}_i^{(t)}, \mathbf{l}_j^{(t)}) - \mu_i|}{\sigma_i}$ ;
- 5 Repeat Lines 2-4 for the node  $j$  to obtain  $Z_j^{(t)}$ ;
- 6 **return**  $-\frac{Z_i^{(t)} + Z_j^{(t)}}{2}$

---

where  $k_i$  is the time step when  $v_i$  first appears. A self-attention mechanism, parameterized by  $\mathbf{W}_Q$ ,  $\mathbf{W}_K$ , and  $\mathbf{W}_V$ , fuses these embeddings to produce a refined representation that captures long-term evolving structural patterns:  $\mathbf{z}_i^{(t)} = \sum_{\mathbf{h}_i^{(\tau)} \in \mathcal{M}_i^{(t)}} \alpha_i^{(\tau)} \mathbf{W}_V \mathbf{h}_i^{(\tau)}$  with  $\alpha_i^{(\tau)} = \frac{\exp((\mathbf{W}_Q \mathbf{h}_i^{(t)})^T (\mathbf{W}_K \mathbf{h}_i^{(\tau)}))}{\sum_{\mathbf{h}_i^{(\tau')} \in \mathcal{M}_i^{(t)}} \exp((\mathbf{W}_Q \mathbf{h}_i^{(t)})^T (\mathbf{W}_K \mathbf{h}_i^{(\tau')}))}$ .

We then measure how much each newly added edge aligns with long-term contextual patterns. For each edge  $(v_i, v_j)$ , we compute its sub-score  $S_L^{(t)}(v_i, v_j) = \sigma(\mathbf{z}_i^{(t)} \mathbf{W}_L \mathbf{z}_j^{(t)} + \mathbf{b}_L)$  by feeding the pair  $(\mathbf{z}_i^{(t)}, \mathbf{z}_j^{(t)})$  into a bilinear layer parameterized by  $\mathbf{W}_L$  and  $\mathbf{b}_L$ , followed by a sigmoid function  $\sigma(\cdot)$ . Notably,  $\mathbf{W}_L$  is constructed as a symmetric matrix to ensure order invariance. Noise-like edges that significantly deviate from long-term contextual patterns are expected to have low sub-scores from  $M_L$ .

### 3.3 Short-term Module $M_S$

The short-term module  $M_S$  captures short-term temporal patterns (e.g., consistency across consecutive time steps) and detects noise-like edges that deviate from these patterns, by computing statistical distances.

To achieve this, we define a consistency score (Algorithm 1) that quantifies how well each incoming edge aligns with existing edges. This consistency score is primarily computed based on latent vectors derived from a surrogate GCN model  $f_S^{(t)}$ . Specifically, at each time step  $t$ , the surrogate GCN model  $f_S^{(t)}$  from the previous time step is applied to the unpurified graph  $\hat{G}^{(t)}$  and node attributes  $X^{(t)}$  to generate a latent matrix  $\mathbf{L}^{(t)} = f_S^{(t)}(\hat{G}^{(t)}, \mathbf{X}^{(t)})$  consisting of latent vectors  $\mathbf{l}_i^{(t)}$  for all the nodes  $v_i$  in  $\hat{G}^{(t)}$ .<sup>5</sup> Using these latent vectors, given an edge  $(v_i, v_j)$ , we first evaluate the latent-vector-based statistics from  $v_i$ 's perspective by statistically comparing  $v_j$ 's latent vector with the latent vectors of  $v_i$ 's neighbors in  $N_i^{(t)}$ . Specifically, we measure KL divergence (Line 2) and then perform

---

<sup>5</sup> We assume the surrogate GCN model  $f_S^{(t)}$  is trained at the previous time step for some downstream task, e.g., node classification. The details of  $f_S^{(t)}$ 's appear in Sec. 4.

a Z-score test by computing the mean  $\mu_i^{(t)}$  and standard deviation  $\sigma_i^{(t)}$  of the KL divergences (Line 3) to obtain the Z-score  $Z_i^{(t)}$  (Line 4). We repeat the same procedure for  $v_j$  (Line 5). Finally, we take the average of those two Z-scores and attach  $(-)$  sign to define the *consistency score* of the edge (Line 6).

The sub-score of  $M_S$  for the edge  $(v_i, v_j)$ , denoted as  $S_S^{(t)}(v_i, v_j)$ , is simply this consistency score. Noise-like edges, which significantly deviate from short-term consistency patterns, are expected to have low sub-scores from  $M_S$ .

### 3.4 Ensemble Module

We employ an ensemble approach to combine the sub-scores from the modules mentioned above. To address the challenge of capturing temporal patterns during the early stages without enough training data accumulated, we incorporate an additional proximity-based sub-score to complement these modules.

The weights for the sub-scores from modules  $M_L$  and  $M_S$  are derived from the corresponding representations/latent vectors,  $\mathbf{z}_i^{(t)}$ 's and  $\mathbf{l}_i^{(t)}$ 's. For each sub-score  $S_L^{(t)}(v_i, v_j)$  from  $M_L$ , the element-wise mean and max of the representations are concatenated:  $\mathbf{x}_L^{(t)}(v_i, v_j) = [\text{elementMean}(\mathbf{z}_i^{(t)}, \mathbf{z}_j^{(t)}) || \text{elementMax}(\mathbf{z}_i^{(t)}, \mathbf{z}_j^{(t)})]$ , where  $||$  denotes vector concatenation. The vector  $\mathbf{x}_L^{(t)}(v_i, v_j)$  is then passed through a two-layer MLP to compute the weight:  $a_L^{(t)}(v_i, v_j) = \text{MLP}_L(\mathbf{x}_L^{(t)}(v_i, v_j))$ . Similarly, the weight  $a_S^{(t)}(v_i, v_j)$  for each sub-score  $S_S^{(t)}(v_i, v_j)$  from  $M_S$  is computed using the latent vectors  $\mathbf{l}_i^{(t)}$ 's. For the proximity-based sub-scores  $S_P^{(t)}(v_i, v_j)$ 's, their weight is a hyperparameter  $w_p$  shared for all edges.

We normalize the weights using softmax, i.e.,  $\hat{\alpha}_L^{(t)}(v_i, v_j)$ ,  $\hat{\alpha}_S^{(t)}(v_i, v_j)$ ,  $\hat{\alpha}_P^{(t)}(v_i, v_j) = \text{softmax}(a_L^{(t)}(v_i, v_j), a_S^{(t)}(v_i, v_j), w_p)$ , and normalize the sub-scores  $S_S^{(t)}$  and  $S_P^{(t)}$  to  $[0, 1]$  using min-max normalization. For each edge  $(v_i, v_j)$ , the *final purification score*  $S^{(t)}(v_i, v_j)$  is the weighted sum of the normalized sub-scores:  $S^{(t)}(v_i, v_j) = \hat{\alpha}_L^{(t)}(v_i, v_j)S_L^{(t)}(v_i, v_j) + \hat{\alpha}_S^{(t)}(v_i, v_j)S_S^{(t)}(v_i, v_j) + \hat{\alpha}_P^{(t)}(v_i, v_j)S_P^{(t)}(v_i, v_j)$ .

### 3.5 Self-supervised Training Procedure

The proposed method, TiGER, employs self-supervised learning to identify noise edges without any ground-truth labels on noise edges, by assigning pseudo-labels to node pairs in the unpurified graph.

At each time step  $t$ , positive pseudo-labels are assigned to all the edges in the unpurified graph  $\hat{G}^{(t)} = (\hat{V}^{(t)}, \hat{E}^{(t)})$ , i.e.,  $T_p = \hat{E}^{(t)}$ , and negative pseudo-labels to randomly selected non-edges, i.e.,  $T_n \subseteq \{(v_i, v_j) \mid (v_i, v_j) \notin \hat{E}^{(t)}\}$ , with  $|T_p| = |T_n|$  for balanced training.

Noise-like edges may also be assigned positive pseudo labels, potentially misleading the training process. To mitigate this, we filter out low-scoring positive pseudo-labels during training, keeping only the top  $\beta\%$  of edges based on the final purification scores  $S^{(t)}(v_i, v_j)$ 's (Sec. 3.4), where  $\beta$  is a hyperparameter. We compute binary cross-entropy loss on the filtered positive sample set  $T_p(\beta)$ :  $\mathcal{L} = -\frac{1}{|T_p(\beta)|} \sum_{(v_i, v_j) \in T_p(\beta)} \log(S^{(t)}(v_i, v_j)) - \frac{1}{|T_n|} \sum_{(v_i, v_j) \in T_n} \log(1 - S^{(t)}(v_i, v_j))$ .

### 3.6 Complexity Analysis

The time complexity of TiGER involves inferring sub-scores from each module and combining them through the ensemble model. At time step  $t$ , consider the unpurified graph  $\hat{G}^{(t)}$  with  $n$  nodes and  $m$  edges. Let  $\bar{k}$  denote the average node degree, and  $\Delta m$  be the number of incoming edges  $\Delta E^{(t)}$ . Let  $d$  represent the dimension of the node features. Assume that the GCNs have  $l$  layers, each with hidden dimensions on the order of  $d$ .

The time complexity of TiGER is dominated by three main operations: (1) GCN inference in both long-term and short-term modules, each with complexity  $O(ld(nd + m))$ ; (2) the long-term self-attention mechanism, which processes one query against historical embeddings per node, with complexity  $O(ntd^2)$ ; and (3) computations for incoming edges, including statistical distances ( $O(\Delta m \bar{k} d)$ ), Adamic-Adar-based proximity sub-scores ( $O(\Delta m \bar{k})$ ), and weights from a two-layer MLP ( $O(\Delta m d^2)$ ). Combining these terms, the total complexity per time step is  $O(ld(nd + m) + ntd^2 + \Delta m(\bar{k}d + \bar{k} + d^2))$ .

These results indicate that complexity of TiGER per time step is linear with respect to the number of nodes  $n$  and the number of edges  $m$ , and the empirical results in Online Appendix [5] further substantiate this analysis.

## 4 Experiments

In this section, we evaluate TiGER to answer the Q1-Q3:

- Q1. **Accuracy**: How accurately does TiGER identify noise edges?
- Q2. **Effectiveness**: How much does TiGER enhance node classification?
- Q3. **Ablation Study**: Does each component of TiGER improve performance?

### 4.1 Experiment Settings

**Datasets.** We use five real-world datasets, comprising (1) three citation graphs: Aminer, Patent, and arXivAI, (2) a friendship graph: School, and (3) a co-authorship graph: DBLP. Some basic statistics of the datasets and details about data pre-processing are provided in Online Appendix [5].

**Noisy time-evolving graph generation.** For numerical evaluation, we introduce noise edges that are not present in the original graph into each dataset. Specifically, at each time step  $t$ , we add noise edges corresponding to 30% of the newly added edges  $\Delta E^{(t)}$  to the graph. These noise edges are sampled uniformly at random from non-adjacent node pairs belonging to different classes. For each dataset, we generate ten noisy graphs, and all results are averaged over them.

**Competitors.** We evaluate TiGER against six competitors, comprising (1) two local similarity-based methods: Adamic-Adar index (A.A.) and Jaccard coefficient (JACCARD), (2) three global similarity-based methods: SVD, GDC [8], and TIARA [9]<sup>6</sup>, and (3) a GNN-based approach: LEO [4]. Details of the competitors can be found in Online Appendix [5].

<sup>6</sup> We adapt GDC [8] and TIARA [9], originally designed for edge augmentation, for graph purification by removing edges with the least similarity or proximity.

**Node classification.** In Sec. 4.3, to evaluate effectiveness, we compare node classification performance on graphs purified by TiGER and its competitors. Specifically, at each time step, a graph convolutional network (GCN) is trained on the purified graph. It is also used as the surrogate GCN model  $f_S^{(t)}$  in the short-term module  $M_S$  (see Sec. 3.3).<sup>7</sup> The nodes are randomly divided into training, validation, and test sets in a 1:1:8 ratio, with the same split maintained across all time steps.

**Hyperparameters.** For TiGER, we select the hyperparameters  $\beta$  and  $w_p$  via grid search over  $\{0.1, 0.2, 0.3\}$ , and  $\{1, 5, 10, 20\}$ , respectively. The hidden dimension of each trainable parameter was set to 64. For all methods, we use the ground-truth purification budget  $K$  for each graph at time step  $t$  (i.e.,  $K = 0.3 \times |\Delta E^t|$ ) to ensure a fair comparison. Detailed search spaces and the selected hyperparameters for all methods are provided in Online Appendix [5].

## 4.2 Q1. Accuracy

In Table 1, we report the proportion of noise edges removed by each method in each dataset and at each time step, under the same purification budget (i.e., the number of removed edges) for all methods. Methods exceeding the six-hour time limit (e.g., TIARA and GDC on the DBLP and arXivAI datasets) are marked as *out of time* (O.O.T.). TiGER consistently outperforms all its competitors in nearly all cases, with purification rates up to 10.2% higher than the second-best method (at  $t = 6$  on School dataset). These results show the effectiveness of TiGER in removing noise edges, preserving the integrity of time-evolving graphs.

## 4.3 Q2. Effectiveness

In Fig. 2, we report the node classification accuracy at each time step on each time-evolving graph purified by each method (see Sec. 4.1 for details on node classification). TiGER consistently leads to performance improvements, ranking first in 23 out of 25 cases and second in the remaining two cases (at  $t = 2$  and  $t = 4$  on the Patent dataset). Notably, using TiGER for purification yields up to 5.3% higher node classification accuracy, compared to using the second-best purification method instead, as shown in Fig. 2(a).

## 4.4 Q3. Ablation Study

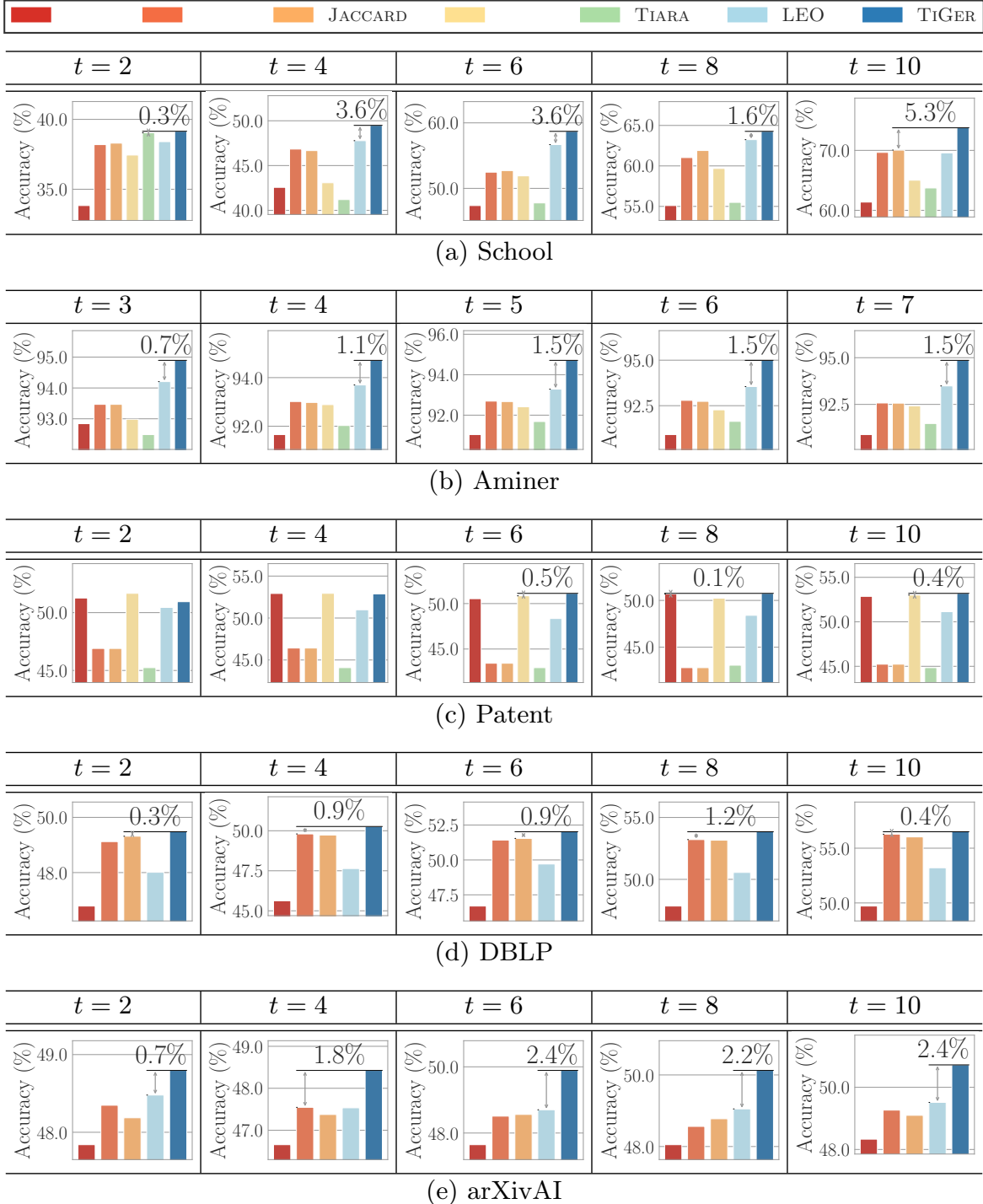
We evaluate the contributions of two key components of TiGER, i.e., the long-term module  $M_L$  and the short-term module  $M_S$ , through an ablation study. To isolate the contribution of  $M_L$ , we removed the self-attention mechanism, while the contribution of  $M_S$  was evaluated by excluding the module entirely from the ensemble model. We compare original TiGER (utilizing both modules) with its three simplified variants (1) without both modules, (2) without  $M_L$ ,

<sup>7</sup> Specifically, the surrogate GCN model  $f_S^{(t)}$  in the short-term module is the GCN that is trained at time step  $t - 1$  for node classification.

Table 1: (Q1) Accuracy. TiGER accurately identifies noise edges. Each entry in a table represents the proportion of noise removed by each method at each time step. Note that all methods are tested under the same purification budget.

	Method	$t = 2$	$t = 4$	$t = 6$	$t = 8$	$t = 10$
School	SVD	58.41 $\pm$ 1.49	43.01 $\pm$ 1.58	39.47 $\pm$ 1.17	37.39 $\pm$ 0.65	36.16 $\pm$ 0.77
	A.A.	73.19 $\pm$ 1.83	63.33 $\pm$ 1.02	60.41 $\pm$ 0.97	62.81 $\pm$ 1.26	64.28 $\pm$ 1.17
	JACCARD	73.26 $\pm$ 1.85	63.12 $\pm$ 1.08	60.29 $\pm$ 1.24	62.68 $\pm$ 1.18	64.33 $\pm$ 1.20
	GDC	66.09 $\pm$ 1.58	53.88 $\pm$ 1.59	50.99 $\pm$ 1.86	49.33 $\pm$ 1.37	47.23 $\pm$ 1.24
	TIARA	62.10 $\pm$ 2.43	45.36 $\pm$ 1.86	38.99 $\pm$ 1.37	38.73 $\pm$ 1.34	38.00 $\pm$ 1.24
	LEO	72.32 $\pm$ 2.40	60.69 $\pm$ 1.30	57.22 $\pm$ 1.34	60.29 $\pm$ 1.25	61.49 $\pm$ 0.84
	TiGER	<b>76.38<math>\pm</math>1.95</b> (+4.3%)	<b>69.46<math>\pm</math>0.89</b> (+9.7%)	<b>66.57<math>\pm</math>0.79</b> (+10.2%)	<b>69.17<math>\pm</math>1.05</b> (+10.1%)	<b>69.84<math>\pm</math>0.91</b> (+8.6%)
Patent	SVD	90.67 $\pm$ 0.42	86.86 $\pm$ 0.42	84.47 $\pm$ 0.28	81.52 $\pm$ 0.46	80.16 $\pm$ 0.52
	A.A.	61.25 $\pm$ 0.69	43.02 $\pm$ 0.52	36.10 $\pm$ 0.53	33.08 $\pm$ 0.38	31.12 $\pm$ 0.37
	JACCARD	61.25 $\pm$ 0.69	43.02 $\pm$ 0.52	36.10 $\pm$ 0.53	33.08 $\pm$ 0.38	31.12 $\pm$ 0.37
	GDC	88.91 $\pm$ 1.60	84.41 $\pm$ 1.06	82.87 $\pm$ 0.84	82.42 $\pm$ 0.75	80.44 $\pm$ 0.80
	TIARA	54.31 $\pm$ 0.38	31.23 $\pm$ 0.33	23.61 $\pm$ 0.36	20.20 $\pm$ 0.33	18.74 $\pm$ 0.29
	LEO	91.87 $\pm$ 0.87	89.67 $\pm$ 0.46	88.74 $\pm$ 0.80	88.30 $\pm$ 0.64	87.48 $\pm$ 0.64
	TiGER	<b>92.25<math>\pm</math>0.72</b> (+0.4%)	<b>89.88<math>\pm</math>0.47</b> (+0.2%)	<b>89.09<math>\pm</math>0.33</b> (+0.4%)	<b>88.61<math>\pm</math>0.28</b> (+0.4%)	<b>87.79<math>\pm</math>0.41</b> (+0.4%)
DBLP	SVD	62.56 $\pm$ 0.12	44.50 $\pm$ 0.22	39.19 $\pm$ 0.13	37.15 $\pm$ 0.18	36.35 $\pm$ 0.15
	A.A.	<u>89.87<math>\pm</math>0.10</u>	84.61 $\pm$ 0.13	84.08 $\pm$ 0.11	84.86 $\pm$ 0.09	85.70 $\pm$ 0.08
	JACCARD	89.87 $\pm$ 0.11	<u>84.68<math>\pm</math>0.15</u>	<u>84.15<math>\pm</math>0.14</u>	<u>84.90<math>\pm</math>0.12</u>	<u>85.73<math>\pm</math>0.10</u>
	GDC	O.O.T.	O.O.T.	O.O.T.	O.O.T.	O.O.T.
	TIARA	O.O.T.	O.O.T.	O.O.T.	O.O.T.	O.O.T.
	LEO	89.29 $\pm$ 0.32	83.12 $\pm$ 0.47	81.56 $\pm$ 0.41	81.28 $\pm$ 0.41	81.28 $\pm$ 0.33
	TiGER	<b>92.34<math>\pm</math>0.12</b> (+2.7%)	<b>88.40<math>\pm</math>0.26</b> (+4.4%)	<b>87.85<math>\pm</math>0.25</b> (+4.4%)	<b>88.21<math>\pm</math>0.25</b> (+3.9%)	<b>88.68<math>\pm</math>0.23</b> (+3.4%)
ArXivAI	SVD	73.28 $\pm$ 0.09	60.54 $\pm$ 0.07	56.44 $\pm$ 0.07	54.98 $\pm$ 0.06	53.85 $\pm$ 0.05
	A.A.	81.07 $\pm$ 0.07	71.66 $\pm$ 0.08	69.39 $\pm$ 0.06	68.72 $\pm$ 0.06	68.50 $\pm$ 0.06
	JACCARD	81.11 $\pm$ 0.06	71.71 $\pm$ 0.08	69.45 $\pm$ 0.07	68.76 $\pm$ 0.07	<u>68.53<math>\pm</math>0.07</u>
	GDC	O.O.T.	O.O.T.	O.O.T.	O.O.T.	O.O.T.
	TIARA	O.O.T.	O.O.T.	O.O.T.	O.O.T.	O.O.T.
	LEO	83.81 $\pm$ 0.35	74.39 $\pm$ 0.22	70.87 $\pm$ 0.23	68.99 $\pm$ 0.28	67.86 $\pm$ 0.24
	TiGER	<b>84.40<math>\pm</math>0.32</b> (+0.7%)	<b>76.24<math>\pm</math>0.24</b> (+2.5%)	<b>73.88<math>\pm</math>0.24</b> (+4.2%)	<b>72.99<math>\pm</math>0.26</b> (+5.8%)	<b>72.61<math>\pm</math>0.25</b> (+6.0%)
	Method	$t = 3$	$t = 4$	$t = 5$	$t = 6$	$t = 7$
Aminer	SVD	60.87 $\pm$ 0.55	49.75 $\pm$ 0.54	41.99 $\pm$ 0.61	37.54 $\pm$ 0.69	34.67 $\pm$ 0.51
	A.A.	67.29 $\pm$ 0.94	59.46 $\pm$ 0.88	54.43 $\pm$ 0.81	52.37 $\pm$ 0.79	50.44 $\pm$ 0.62
	JACCARD	67.29 $\pm$ 0.94	59.43 $\pm$ 0.84	54.43 $\pm$ 0.81	52.32 $\pm$ 0.79	50.43 $\pm$ 0.64
	GDC	64.33 $\pm$ 1.02	55.83 $\pm$ 1.10	49.80 $\pm$ 0.97	45.87 $\pm$ 0.91	43.89 $\pm$ 0.84
	TIARA	63.00 $\pm$ 0.85	51.66 $\pm$ 0.71	44.73 $\pm$ 0.66	41.00 $\pm$ 0.57	39.13 $\pm$ 0.57
	LEO	82.70 $\pm$ 0.88	78.50 $\pm$ 0.90	75.55 $\pm$ 0.84	74.07 $\pm$ 0.88	73.40 $\pm$ 0.89
	TiGER	<b>84.21<math>\pm</math>1.27</b> (+1.8%)	<b>80.86<math>\pm</math>1.53</b> (+3.0%)	<b>79.17<math>\pm</math>1.30</b> (+4.8%)	<b>78.74<math>\pm</math>1.01</b> (+6.3%)	<b>78.28<math>\pm</math>0.98</b> (+6.6%)

Fig. 2: (Q2) Effectiveness. TiGER consistently enhances node classification performance, outperforming its competitors in most cases. On the DBLP and ArXivAI datasets, GDC and TIARA exceed the six-hour time limit.



and (3) without  $M_S$ . As shown in Table 2, where the ArXivAI dataset is used, integrating both modules significantly improves noise identification accuracy.

Table 2: (Q3) Ablation Study. TiGER achieves better purification accuracy than its variants, highlighting the complementary contributions of its long-term module ( $M_L$ ) and its short-term module ( $M_S$ ). Each entry represents the proportion of noise purified by each method at each time step in the ArXivAI dataset.

$M_L$	$M_S$	$t = 2$	$t = 4$	$t = 6$	$t = 8$	$t = 10$
✗	✗	83.73±0.27	74.51±0.36	71.07±0.26	69.35±0.34	68.29±0.33
✗	✓	83.95±0.20	74.79±0.30	71.57±0.33	69.73±0.35	68.66±0.35
✓	✗	84.33±0.24	76.16±0.20	73.77±0.21	72.64±0.22	71.95±0.25
✓	✓	<b>84.40±0.32</b>	<b>76.24±0.24</b>	<b>73.88±0.24</b>	<b>72.99±0.26</b>	<b>72.61±0.25</b>

## 5 Conclusions

In this paper, we proposed TiGER, a self-supervised method for purifying time-evolving graphs. By leveraging dedicated modules to capture long-term patterns and short-term patterns, TiGER identifies and filters out noise edges that deviate from these temporal patterns. Its proximity-based ensemble strategy further enhances robustness. Our extensive experiments showed that TiGER consistently outperforms its competitors in noise purification and downstream node classification. For reproducibility, we provide our code and datasets at [5].

**Acknowledgements.** This work was supported by Institute of Information & communications Technology Planning & Evaluation (IITP) grant funded by the Korea government (MSIT) (No. RS-2024-00457882, AI Research Hub Project, 50%) (No. No. 2022-0-00157/RS-2022-II220157, Robust, Fair, Extensible Data-Centric Continual Learning, 40%) (RS-2019-II190075, Artificial Intelligence Graduate School Program (KAIST), 10%).

## References

1. Barros, C.D., Mendonça, M.R., Vieira, A.B., Ziviani, A.: A survey on embedding dynamic graphs. *ACM Computing Surveys* **55**(1), 1–37 (2021)
2. Chen, D., Lin, Y., Li, W., Li, P., Zhou, J., Sun, X.: Measuring and relieving the over-smoothing problem for graph neural networks from the topological view. In: *AAAI* (2020)
3. Entezari, N., Al-Sayouri, S.A., Darvishzadeh, A., Papalexakis, E.E.: All you need is low (rank) defending against adversarial attacks on graphs. In: *WSDM* (2020)
4. Jo, H., Hwang, H., Bu, F., Lee, S.Y., Park, C., Shin, K.: On measuring unnoticeability of graph adversarial attacks: Observations, new measure, and applications. In: *KDD* (2025)
5. Jo, H., Lee, J., Bu, F., Shin, K.: Tiger: Self-supervised purification for time-evolving graphs: Online appendix and code. <https://github.com/HyeonsooJo/TiGER> (2025)
6. Kang, Z., Pan, H., Hoi, S.C., Xu, Z.: Robust graph learning from noisy data. *IEEE transactions on cybernetics* **50**(5), 1833–1843 (2019)

7. Kazemi, S.M., Goel, R., Jain, K., Kobyzev, I., Sethi, A., Forsyth, P., Poupart, P.: Representation learning for dynamic graphs: A survey. *Journal of Machine Learning Research* **21**(70), 1–73 (2020)
8. Klicpera, J., Weißenberger, S., Günnemann, S.: Diffusion improves graph learning. In: *NeurIPS* (2019)
9. Lee, J.w., Jung, J.: Time-aware random walk diffusion to improve dynamic graph learning. In: *AAAI* (2023)
10. Lee, J., Kim, S., Shin, K.: Slade: Detecting dynamic anomalies in edge streams without labels via self-supervised learning. In: *KDD* (2024)
11. Li, H., Li, C., Feng, K., Yuan, Y., Wang, G., Zha, H.: Robust knowledge adaptation for dynamic graph neural networks. *IEEE Transactions on Knowledge and Data Engineering* **36**(11), 6920–6933 (2024)
12. Luo, D., Cheng, W., Yu, W., Zong, B., Ni, J., Chen, H., Zhang, X.: Learning to drop: Robust graph neural network via topological denoising. In: *WSDM* (2021)
13. Pareja, A., Domeniconi, G., Chen, J., Ma, T., Suzumura, T., Kanezashi, H., Kaler, T., Schardl, T., Leiserson, C.: Evolvegcn: Evolving graph convolutional networks for dynamic graphs. In: *AAAI* (2020)
14. Rossi, E., Chamberlain, B., Frasca, F., Eynard, D., Monti, F., Bronstein, M.: Temporal graph networks for deep learning on dynamic graphs. In: *ICML Workshop on Graph Representation Learning* (2020)
15. Sankar, A., Wu, Y., Gou, L., Zhang, W., Yang, H.: Dysat: Deep neural representation learning on dynamic graphs via self-attention networks. In: *WSDM* (2020)
16. Sathre, P., Gondhalekar, A., Feng, W.c.: Edge-connected jaccard similarity for graph link prediction on fpga. In: *HPEC* (2022)
17. Shen, X., Lio, P., Yang, L., Yuan, R., Zhang, Y., Peng, C.: Graph rewiring and preprocessing for graph neural networks based on effective resistance. *IEEE Transactions on Knowledge and Data Engineering* **36**(11), 6330–6343 (2024)
18. Skarding, J., Gabrys, B., Musial, K.: Foundations and modeling of dynamic networks using dynamic graph neural networks: A survey. *IEEE Access* **9**(1), 79143–79168 (2021)
19. Spinelli, I., Scardapane, S., Hussain, A., Uncini, A.: Fairdrop: Biased edge dropout for enhancing fairness in graph representation learning. *IEEE Transactions on Artificial Intelligence* **3**(3), 344–354 (2021)
20. Tian, H., Zafarani, R.: Exploiting common neighbor graph for link prediction. In: *CIKM* (2020)
21. Tian, S., Wu, R., Shi, L., Zhu, L., Xiong, T.: Self-supervised representation learning on dynamic graphs. In: *CIKM* (2021)
22. Vaswani, A., Shazeer, N., Parmar, N., Uszkoreit, J., Jones, L., Gomez, A.N., Kaiser, Ł., Polosukhin, I.: Attention is all you need. In: *NeurIPS* (2017)
23. Xu, M., Zhang, B., Yuan, J., Cao, M., Wang, C.: Ned-gnn: Detecting and dropping noisy edges in graph neural networks. In: *APWeb* (2022)
24. Yu, W., Cheng, W., Aggarwal, C., Chen, H., Wang, W.: Link prediction with spatial and temporal consistency in dynamic networks. In: *IJCAI* (2017)
25. Zhang, S., Xiong, Y., Zhang, Y., Sun, Y., Chen, X., Jiao, Y., Zhu, Y.: Rdgsl: Dynamic graph representation learning with structure learning. In: *CIKM* (2023)
26. Zhu, W., Ruan, K., Huang, J., Xiao, J., Yu, W.: Dynamic graph representation based on temporal and contextual contrasting. In: *ACAI* (2022)

# Online Appendix

## A Details of Experiment Settings

Table 1: Summary of the real-world datasets

Name	# Nodes	# Edges	# time steps	# Classes	Summary
School [?]	319	2,327	10	9	Friendship
Aminer [?]	3,111	7,995	7	4	Citation
Patent [?]	12,214	41,916	10	6	Citation
DBLP [?]	28,085	150,568	10	10	Co-author
arXivAI [?]	69,854	696,819	10	5	Citation

### A.1 Details of Datasets

We use five real-world time-evolving graph datasets of various types:

- *Aminer* and *arXivAI* are citation networks where nodes represent publications, and edges denote citation links between them.
- *Patent* is a patent citation network, where nodes represent patents, and edges indicate citation relationships among them.
- *School* is a friendship network where nodes represent students, and edges denote friendship interactions.
- *DBLP* is a co-authorship network, where nodes represent authors, and edges indicate co-authorship relationships between them.

Since these datasets do not provide node features, we generated 128-dimensional embeddings for node features by applying positional encoding based on the order in which the nodes appeared. To construct the time-evolving graphs, we processed the datasets to ensure that the number of incoming edges at each time step is equal. In this process, the Patent dataset was divided into a total of 7 time steps, while the remaining datasets were divided into 10 time steps each.

### A.2 Details of TiGER

The GCN  $f_L^{(t)}$  in  $M_L$  and  $f_S^{(t)}$  in  $M_S$  are both 2-layer networks. The hidden dimension for each module is set to 64. For the proximity score additionally used in the ensemble, we employed SVD for the Patent dataset and the A.A. for the

other datasets. The learning rate was searched within the range  $\{1e-3, 5e-3, 1e-2, 5e-2\}$ . The hyperparameters  $\beta$  and  $w_p$  were selected via grid search over  $\{0.1, 0.2, 0.3\}$  and  $\{1, 5, 10, 20\}$ , respectively. The model was trained for 100 epochs. Positive and negative pseudo-labeled edges were randomly divided in a 4:1 ratio and used for training and validation, respectively.

### A.3 Details of Competitors

In this section, we provide descriptions of the competitors used in Sec. 4 and introduce their detailed parameter settings.

For a given pair of nodes, JACCARD is defined as the ratio of the number of common neighbors to the total number of neighbors. In the case of the A.A., it is computed as the sum of the inverse degrees of the common neighbors of the given two nodes. SVD uses a rank-100 approximation of the adjacency matrix, where the similarity score of an edge is determined by the corresponding element in the approximated adjacency matrix. GDC employs graph diffusion based on personalized PageRank (PPR). The diffusion matrix (i.e., the output of GDC) is initially degree-normalized. To compute the similarity scores, this diffusion matrix is denormalized, and the element corresponding to each edge in the denormalized diffusion matrix is used as the similarity score for that edge. The teleport probability  $\alpha$ , a hyperparameter for PPR, was selected via grid search over  $\{0.05, 0.1, 0.15, 0.2\}$ , as suggested in the original paper. TIARA extends GDC by incorporating temporal dependencies into the diffusion matrix. Specifically, it computes the diffusion matrix for a given time step as a weighted summation of the current diffusion matrix and those from previous time steps. Like GDC, TIARA also uses PPR-based graph diffusion, and the final similarity score for an edge is determined by the corresponding element in the denormalized diffusion matrix. An additional hyperparameter,  $\beta$ , which controls the weight of the diffusion matrix from previous time steps, was selected via grid search over  $\{0.2, 0.4, 0.6, 0.8\}$ .

## B Scalability of TiGER

We evaluated the scalability of TiGER by measuring how its runtime changes depending on the size of the input graph. To this end, we measured the time required to purify the unpurified graph at each time step for the DBLP and arXivAI datasets. As shown in Fig. 1, **TiGER scaled linearly with the size of the input graph**, as described in Sec. 3.6.

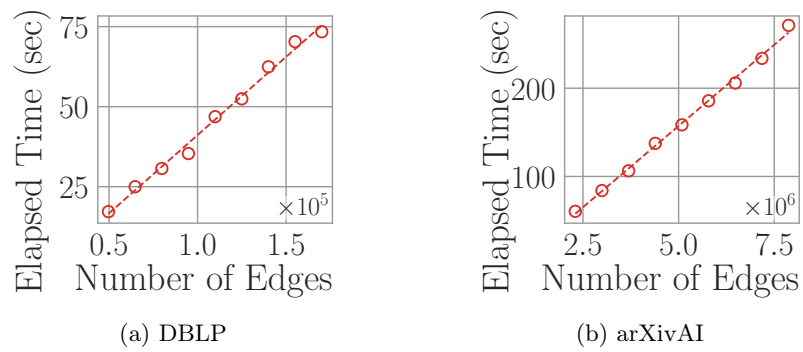


Fig. 1: TiGER scaled **linearly** with the number of edges in the input graph.